

# Multiple superconducting gap and anisotropic spin fluctuations in iron arsenides: Comparison with nickel analog

Z. Li<sup>a</sup>, S. Kawasaki<sup>b</sup>, T. Oka<sup>b</sup>, T. Tabuchi<sup>b</sup>, Y. Ooe<sup>b</sup>, M. Ichioka<sup>b</sup>, Z. A. Ren<sup>a</sup>, Z. X. Zhao<sup>a</sup>, J. L. Luo<sup>a</sup>, N. L. Wang<sup>a</sup>, X. C. Wang<sup>a</sup>, Q. Q. Liu<sup>a</sup>, C. Q. Jin<sup>a</sup>, C.T. Lin<sup>c</sup>, Guo-qing Zheng<sup>a,b</sup>

<sup>a</sup>Institute of Physics and Beijing National Lab for Condensed Matter Physics, Chinese Academy of Science, Beijing, 100190, China

<sup>b</sup>Department of Physics, Okayama University, Okayama 700-8530, Japan

<sup>c</sup>Max Planck Institute, Heisenbergstrasse 1, D-70569 Stuttgart, Germany

## Abstract

We present extensive  $^{75}\text{As}$  NMR and NQR data on the superconducting arsenides  $\text{PrFeAs}_{0.89}\text{F}_{0.11}$  ( $T_c=45$  K),  $\text{LaFeAsO}_{0.92}\text{F}_{0.08}$  ( $T_c=27$  K),  $\text{LiFeAs}$  ( $T_c = 17$  K) and  $\text{Ba}_{0.72}\text{K}_{0.28}\text{Fe}_2\text{As}_2$  ( $T_c = 31.5$  K) single crystal, and compare with the nickel analog  $\text{LaNiAsO}_{0.9}\text{F}_{0.1}$  ( $T_c=4.0$  K). In contrast to  $\text{LaNiAsO}_{0.9}\text{F}_{0.1}$  where the superconducting gap is shown to be isotropic, the spin lattice relaxation rate  $1/T_1$  in the Fe-arsenides decreases below  $T_c$  with no coherence peak and shows a step-wise variation at low temperatures. The Knight shift decreases below  $T_c$  and shows a step-wise  $T$  variation as well. These results indicate spin-singlet superconductivity with multiple gaps in the Fe-arsenides. The Fe antiferromagnetic spin fluctuations are anisotropic and weaker compared to underdoped copper-oxides or cobalt-oxide superconductors, while there is no significant electron correlations in  $\text{LaNiAsO}_{0.9}\text{F}_{0.1}$ . We will discuss the implications of these results and highlight the importance of the Fermi surface topology.

**Keywords:** superconductivity, iron arsenide, nickel arsenide, NMR

## 1. Introduction

The recent discovery of superconductivity in  $\text{LaFeAsO}_{1-x}\text{F}_x$  at the transition temperature  $T_c = 26$  K [1] has attracted great attention. Soon after the initial work,  $T_c$  was raised to 55 K in  $\text{SmFeAsO}_{1-x}\text{F}_x$  [2], which is the highest among materials except cuprates. These compounds have a  $\text{ZrCuSiAs}$  type structure (P4/nmm) in which FeAs forms a two-dimensional network similar to the  $\text{CuO}_2$  plane in the cuprates case. By replacing O with F, *electrons* are doped. After the discovery of  $\text{ReFeAsO}$  (Re: rare earth, so-called 1111 compound), several other Fe-pnictides have been found to superconduct.  $\text{BaFe}_2\text{As}_2$  (so-called 122 compound) has a  $\text{ThCr}_2\text{Si}_2$ -type structure. By replacing Ba with K, *holes* are doped and  $T_c$  can be as high as 38 K [3]. Another arsenide,  $\text{LiFeAs}$  (so-called 111 compound) which has  $\text{Cu}_2\text{Sb}$  type tetragonal structure, was discovered to show superconductivity even in stoichiometric composition[4]. The common feature of these three systems are the iron arsenide plane which dominates the properties of these compounds and hosts the superconductivity.

We have used nuclear magnetic resonance (NMR) and nuclear quadrupole resonance (NQR) techniques to study the pairing symmetry and spin fluctuations in the normal state. We find that these superconductors are in the spin-singlet state with multiple gaps, and the latter property is quite different from the cuprate case. The antiferromagnetic spin fluctuation is weaker than the cuprates and are anisotropic in the spin space.

## 2. Experiments

The preparation of the samples of  $\text{PrFeAs}_{0.89}\text{F}_{0.11}$  ( $T_c=45$  K),  $\text{LaFeAsO}_{0.92}\text{F}_{0.08}$  ( $T_c=23$  K),  $\text{LiFeAs}$  ( $T_c = 17$  K),  $\text{LaNiAsO}_{0.9}\text{F}_{0.1}$  ( $T_c = 4.0$  K), and single crystal  $\text{Ba}_{0.72}\text{K}_{0.28}\text{Fe}_2\text{As}_2$  ( $T_c = 31.5$  K) are published elsewhere [5, 6, 4, 7, 8]. NQR and NMR measurements were carried out by using a phase coherent spectrometer. The NMR spectra were taken by sweeping the magnetic field at a fixed frequency. The spin-lattice relaxation rate  $1/T_1$  was measured by using a single saturation pulse.

## 3. Results and Discussion

### 3.1. Knight shift

Figure 1 shows the temperature dependence of the Knight shift for  $\text{PrFeAs}_{0.89}\text{F}_{0.11}$  ( $T_c=45$  K) with the magnetic field ( $H$ ) applied along the *ab*-direction [9]. The shift decreases below  $T_c$  and goes to zero at the  $T=0$  limit. The Knight shift of  $\text{Ba}_{0.72}\text{K}_{0.28}\text{Fe}_2\text{As}_2$  with  $H$  parallel to the *c*-axis [10] also decreases below  $T_c$ , as seen in Fig. 2. The behavior is quite similar to the  $\text{PrFeAs}_{0.89}\text{F}_{0.11}$  case. These results indicate spin-singlet superconductivity.

However, the detailed  $T$  variation of the Knight shift is different from that seen in usual spin-singlet superconductors such as copper-oxides, where  $K$  decreases rapidly below  $T_c$  which is followed by a milder decrease at low temperatures, as illustrated by the broken curve in Fig. 1. In contrast, the decrease of the Knight shift shows a step-wise behavior at a temperature about half the  $T_c$ .

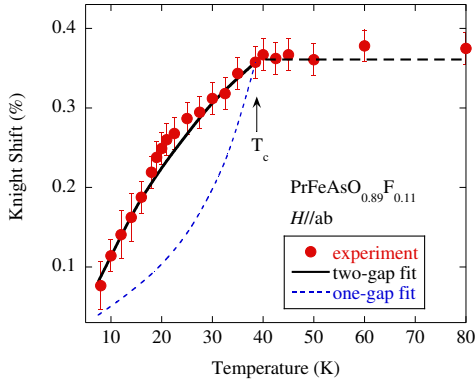


Figure 1: (color online) The temperature variation of  $^{75}\text{As}$  Knight shift of  $\text{PrFeAsO}_{0.89}\text{F}_{0.11}$  with  $H \parallel ab$ . The solid curve is a fitting of two  $d$ -wave gaps with  $\Delta_1(T=0) = 3.5k_B T_c$  and a relative weight of 0.4, and  $\Delta_2(T=0) = 1.1k_B T_c$  with a relative weight of 0.6 (see text). The broken curve below  $T_c$  is a simulation for the larger gap alone.

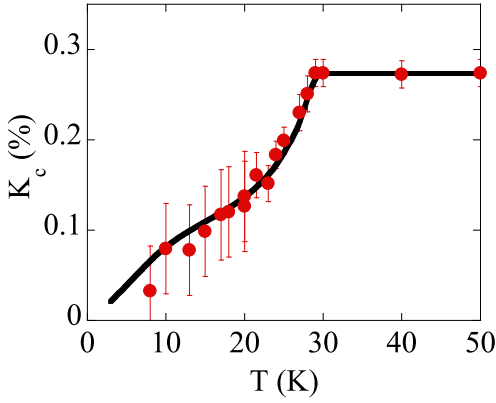


Figure 2: (color online) The Knight shift data of  $\text{Ba}_{0.72}\text{K}_{0.28}\text{Fe}_2\text{As}_2$  with  $H \parallel c$ -axis. The arrow indicates  $T_c$ . The curve below  $T_c$  is a fit to a two-gap model (see text).

### 3.2. $T_1$ in the superconducting state

The step-wise decrease of the Knight shift is also reflected in the temperature dependence of the  $^{19}\text{F}$  spin-lattice relaxation rate  $1/T_1$  [9], and is also seen in  $\text{LaFeAsO}_{0.92}\text{F}_{0.08}$  ( $T_c=23$  K)[11] and the hole-doped  $\text{Ba}_{0.72}\text{K}_{0.28}\text{Fe}_2\text{As}_2$  ( $T_c=31.5$  K)[10]. Figure 3 shows the temperature dependence of  $1/T_1$  measured by  $^{19}\text{F}$  NMR in  $\text{PrFeAsO}_{0.89}\text{F}_{0.11}$  ( $T_c = 45$  K), and Fig. 4 shows the temperature dependence of  $1/T_1$  measured by  $^{75}\text{As}$  NQR in  $\text{LaFeAsO}_{0.92}\text{F}_{0.08}$  ( $T_c=23$  K). Below  $T_c$ , there is no coherence peak for both samples. Moreover, a bending feature is seen around  $T \sim T_c/2$  [9, 11]. This behavior is not expected in a single-gap superconductor.

Figure 5 shows the temperature dependence of  $1/T_1$  measured by  $^{75}\text{As}$  NMR with the magnetic field applied along the  $c$ -axis in  $\text{Ba}_{0.72}\text{K}_{0.28}\text{Fe}_2\text{As}_2$  ( $T_c = 31.5$  K) single crystal [10].  $1/T_1$  also shows a "knee"-shape around  $T \sim T_c/2$ . Namely, the sharp drop of  $1/T_1$  just below  $T_c$  is gradually replaced by a slower change below  $T \sim 15$  K, then followed by another steeper drop below. This "convex" shape is clearly different from the case of superconductors with a single gap which shows

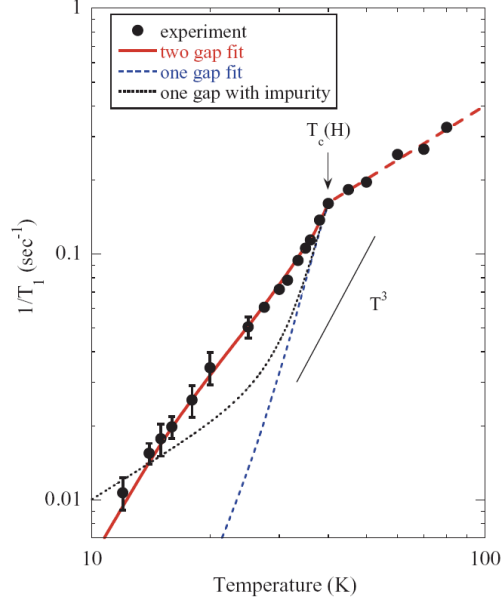


Figure 3: (color online) The temperature dependence of  $^{19}\text{F}$  spin-lattice relaxation rate  $1/T_1$  in  $\text{PrFeAs}_{0.89}\text{F}_{0.11}$  measured at  $\mu_0 H = 1.375$  T. The broken line indicates a relation of  $T_1 T = \text{const}$  which holds for a weakly correlated electron system. The thin straight line illustrates the temperature dependence of  $T^3$ .

a "concave" shape of  $T$ -variation.

We find that a two-gap model can reproduce the step-wise  $T$  variation of  $1/T_1$  and the Knight shift. The underlying physics is that the system is dominantly governed by a larger gap for  $T$  near  $T_c$  while at sufficiently low  $T$  it starts to "notice" the existence of a smaller gap, resulting in another drop in  $1/T_1$  below  $T \sim T_c/2$ . In the  $d$ -wave case with two gaps, where the density of states (DOS) is  $N_{s,i}(E) = N_{0,i} \frac{E}{\sqrt{E^2 - \Delta_i^2}}$ , the Knight shift and  $1/T_{1s}$  in the superconducting state are written as

$$\frac{K_s}{K_N} = \int N_s(E) \frac{\partial f(E)}{\partial E} dE \quad (1)$$

$$\frac{T_{1N}}{T_{1s}} = \sum \frac{2}{k_B T} \int \int N_{s,i}(E) N_{s,i}(E') f(E) [1 - f(E')] \delta(E - E') dE dE' \quad (2)$$

where  $f(E)$  is the Fermi distribution function. We find that the parameters  $2\Delta_1(0) = 7.0k_B T_c$ ,  $2\Delta_2(0) = 2.2k_B T_c$  and  $\kappa = 0.4$  can fit the data of both the shift and  $1/T_1$  very well, as shown by the solid curves in Fig. 1 and Fig. 3, where

$$\kappa = \frac{N_{0,1}}{N_{0,1} + N_{0,2}} \quad (3)$$

is the relative DOS of the band(s) with larger gap to the total DOS.

Application of the same model to  $\text{LaFeAsO}_{0.92}\text{F}_{0.08}$  gives  $2\Delta_1(0) = 8.4k_B T_c$ ,  $2\Delta_2(0) = 3.2k_B T_c$ , and  $\kappa = 0.6$  [11]. On the other hand, for  $\text{Ba}_{0.72}\text{K}_{0.28}\text{Fe}_2\text{As}_2$ ,  $2\Delta_1(0) = 9.0k_B T_c$ ,  $2\Delta_2(0) = 1.62k_B T_c$ , and  $\kappa = 0.69$  was obtained [10]. The same model can also fit the Knight shift data, as seen in Fig. 2.

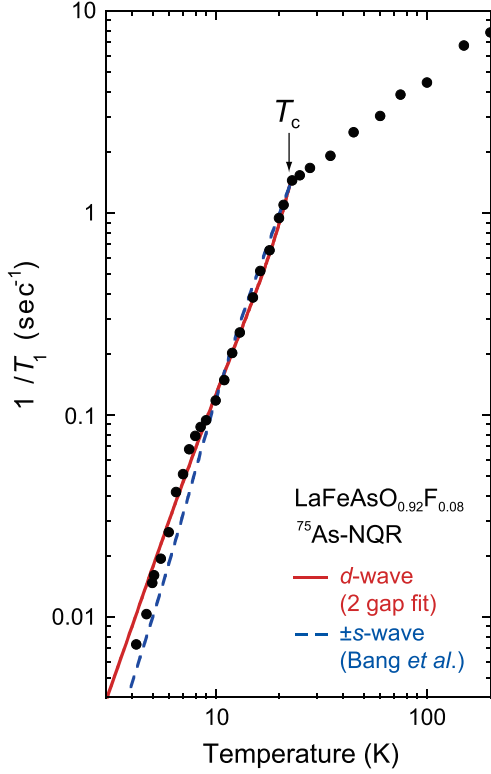


Figure 4: (color online)  $^{75}\text{As}$  ( $1/T_1$ ) in  $\text{LaFeAsO}_{0.92}\text{F}_{0.08}$ . The solid curve is a two gap fit assuming a  $d$ -wave symmetry with parameters,  $\Delta_1(0) = 4.2k_B T_c$ ,  $\Delta_2(0) = 1.6k_B T_c$ , and  $\kappa = 0.6$  (see text). The dotted curve is a simulation assuming two  $s$ -wave gaps that change signs with parameters,  $\Delta_1(0) = 3.75k_B T_c$ ,  $\Delta_2(0) = 1.5k_B T_c$ , and  $\kappa = 0.38$ .

For the case of  $s^\pm$ -gap [12, 13], recent calculations have shown that scattering between the different bands may reduce the coherence peak just below  $T_c$  [14, 15]. Following Ref.[15], we calculated  $1/T_1$  for the  $s^\pm$ -gap model, by introducing the impurity scattering parameter  $\eta$  in the energy spectrum,  $E = \omega + i\eta$ . The parameters  $2\Delta_1(0) = 7.5k_B T_c$ ,  $2\Delta_2(0) = 3.0k_B T_c$ ,  $\kappa = 0.38$  and  $\eta = 0.15k_B T_c$ , can well fit the data, as shown in Fig. 4. where

$$\eta = \frac{\pi n_{\text{imp}}(N_1 + N_2)V^2}{1 + \pi^2(N_1 + N_2)^2 V^2} \quad (4)$$

In the equation,  $n_{\text{imp}}$  is the impurity concentration and  $V$  is the scattering potential at the impurity. A similar set of parameters ( $2\Delta_1(0) = 7.2k_B T_c$ ,  $2\Delta_2(0) = 1.68k_B T_c$ ,  $\kappa = 0.6$  and  $\eta = 0.22k_B T_c$ ) can fit the data of  $\text{Ba}_{0.72}\text{K}_{0.28}\text{Fe}_2\text{As}_2$ , see Fig. 5.

The results for  $\text{LiFeAs}$ [16] (Fig. 6) are shown in Fig. 6. We measured two  $\text{Li}_x\text{FeAs}$  samples with nominal  $x = 0.8$  and  $1.1$ . The physical properties including the NMR results are the same. This supports that only stoichiometric compound can be formed.[17]  $1/T_1$  below  $T_c$  shows a qualitatively similar behavior as the previous three samples, but the behavior at low temperatures is a little different. Namely,  $1/T_1$  becomes to be proportional to  $T$  below  $T \leq T_c/4$ , which indicates that a finite DOS is induced by the impurity scattering. Obviously, this would occur in a  $d$ -wave case. On the other hand, it is also possible in the  $s^\pm$  case provided that the scattering between the electron- and hole-pocket is strong. Calculation by the  $s^\pm$ -

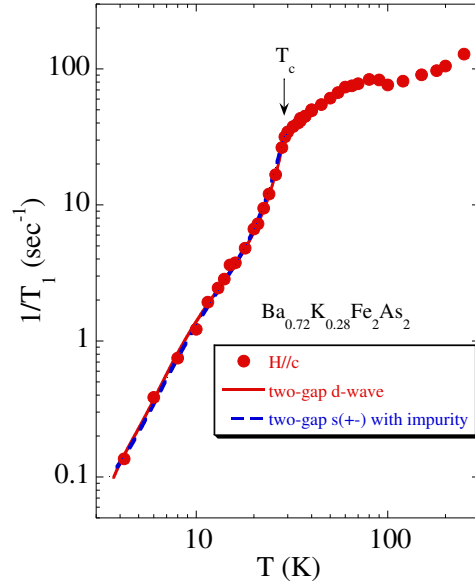


Figure 5: (color online)  $T$ -dependence of  $1/T_1$  in  $\text{Ba}_{0.72}\text{K}_{0.28}\text{Fe}_2\text{As}_2$ . The curves below  $T_c$  (indicated by the arrow) are fits to two-gap models (see text).

wave model shows that the gap value of  $\text{LiFeAs}$  is smaller than other compounds, but the impurity scattering is much larger ( $\eta = 0.26k_B T_c$ ) [16]. The gap parameters for all Fe-arsenide samples are summarized in Tab. 1. To summarize, the multiple gap feature is universal to all Fe-arsenides, which probably associated with the multiple electronic bands [18].

By strong contrast, the nickel analog of  $\text{LaFeAsO}_{1-x}\text{F}_x$ , namely,  $\text{LaNiAsO}_{0.9}\text{F}_{0.1}$  has different behavior.[19] As seen in Fig. 7,  $1/T_1$  shows a well-defined coherence peak just below  $T_c$ , which is a finger print of superconductors with an isotropic gap. This is in sharp contrast to various Fe-arsenides reported so far[9, 11, 10, 20, 21, 22]. At low temperatures,  $1/T_1$  decreases as an exponential function of  $T$ . The solid curves in Fig. 7 are calculations using the BCS model. Following Hebel [23], we convolute  $N_s(E)$  with a broadening function  $B(E)$  which is approximated with a rectangular function centered at  $E$  with a height of  $1/2\delta$ . The solid curves below  $T_c$  shown in Fig. 7 is calculation with  $2\Delta(0) = 3.2k_B T_c$  and  $r \equiv \Delta(0)/\delta = 5$ . Such  $T$ -dependence of  $1/T_1$  in the superconducting state is in striking contrast to that for Fe-arsenide where no coherence peak was observed and the  $T$ -dependence at low- $T$  does not show an exponential behavior. The striking difference may be ascribed to the different topology of the Fermi surfaces. For Fe-arsenides, it has been proposed that  $d$ -wave [24, 25] or sign reversal  $s$ -wave gap [12, 13] can be stabilized due to nesting by the connecting wave vector  $Q = (\pi, 0)$ . In  $\text{LaNiAsO}_{0.9}\text{F}_{0.1}$ , however, there is no such Fermi surface nesting [26], and thus the mechanism for the proposed gap symmetry does not exist. Given that the  $T_c$  is much lower in  $\text{LaNiAsO}_{1-x}\text{F}_x$ , our result suggests the important role of the Fermi-surface topology in the superconductivity of Fe-arsenides.

Finally, for comparison,  $1/T_1$  normalized by the value at  $T_c$  are shown in Fig. 8 as a function of reduced temperature for all

Table 1: The gap parameters.  $\kappa = N_1/(N_1 + N_2)$ ,  $\eta = \frac{\pi n_{\text{imp}}(N_1 + N_2)V^2}{1 + \pi^2(N_1 + N_2)^2 V^2}$ , where  $n_{\text{imp}}$  is the impurity concentration and  $V$  is the scattering potential at the impurity.

	<i>d</i> -wave			<i>s</i> <sup>±</sup> -wave			
	$\Delta_1/k_B T_c$	$\Delta_2/k_B T_c$	$\kappa$	$\Delta_1/k_B T_c$	$\Delta_2/k_B T_c$	$\kappa$	$\eta/k_B T_c$
PrFeAsO <sub>0.89</sub> F <sub>0.11</sub>	3.5	1.1	0.4				
LaFeAsO <sub>0.92</sub> F <sub>0.08</sub>	4.2	1.6	0.6	3.75	1.5	0.38	0.15
Ba <sub>0.72</sub> K <sub>0.28</sub> Fe <sub>2</sub> As <sub>2</sub>	4.5	0.81	0.69	3.6	0.84	0.6	0.22
LiFeAs				3.0	1.3	0.5	0.26

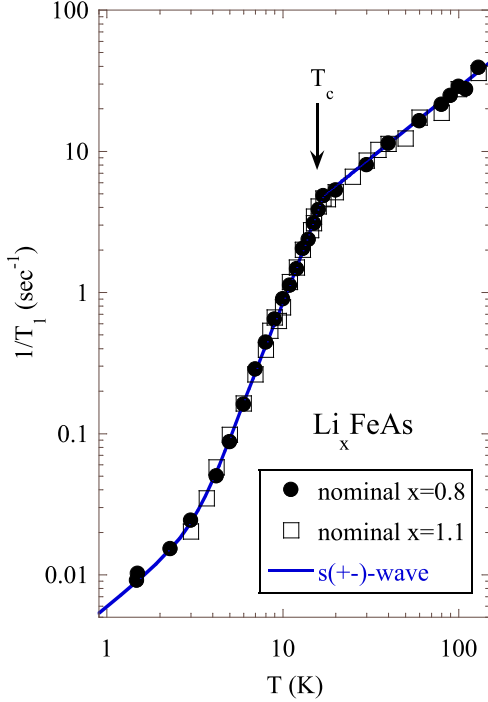


Figure 6: (color online) The  $T$ -dependence of  $1/T_1$  measured by NQR for Li<sub>0.8</sub>FeAs and Li<sub>1.1</sub>FeAs. The curves below  $T_c$  are fits to the  $s^\pm$ -wave model with  $\Delta_1^+ = 3.0 k_B T_c$ ,  $\Delta_2^- = 1.3 k_B T_c$ , and the impurity scattering rate  $\eta = 0.26 k_B T_c$  (see text).

samples.

### 3.3. Normal state properties

Next, we discuss on the character of spin fluctuations. Figure 9 shows the temperature variation of  $1/T_1 T$  in Ba<sub>0.72</sub>K<sub>0.28</sub>Fe<sub>2</sub>As<sub>2</sub>. One notices that, in the normal state above  $T_c$ ,  $1/T_1 T$  increases with decreasing  $T$ , which is an indication of antiferromagnetic electron correlation, since both  $K^a$  and  $K^c$  slightly decrease with decreasing  $T$ , but becomes a constant below  $T \sim 70$  K [10], which resembles closely the cuprate [27] or cobaltate cases [28].

Figure 10 compares  $1/T_1 T$  for four samples. The data for LaFeAsO<sub>0.92</sub>F<sub>0.08</sub>, LiFeAs, LaNiAsO<sub>0.9</sub>F<sub>0.1</sub> are measured by NQR, which correspond to  $H \parallel c$ -axis, since the principle axis of the NQR tensors is along the  $c$ -axis. The data for Ba<sub>0.72</sub>K<sub>0.28</sub>Fe<sub>2</sub>As<sub>2</sub> is measured by NMR with  $H \parallel c$ -axis. The  $1/T_1 T$  of hole-doped Ba<sub>0.72</sub>K<sub>0.28</sub>Fe<sub>2</sub>As<sub>2</sub> increase with decreasing temperature as discussed above. The electron-doped LaFeAsO<sub>0.92</sub>F<sub>0.08</sub> also show similar behavior, although

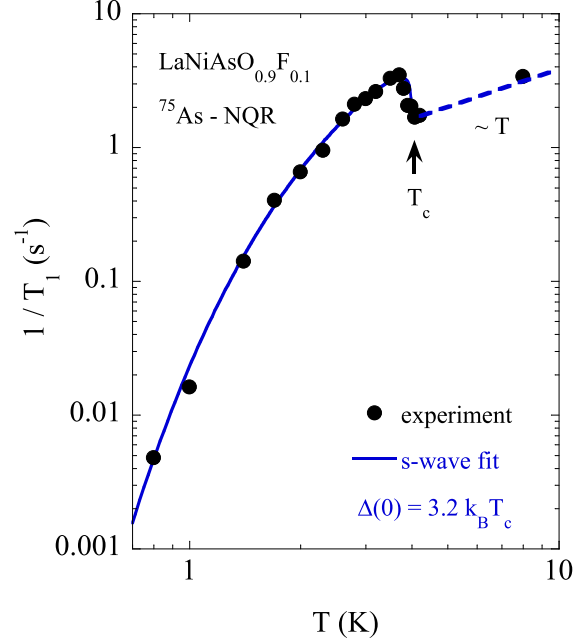


Figure 7: (color online) The  $T$  dependence of the spin lattice relaxation rate,  $1/T_1$ , for LaNiAsO<sub>0.9</sub>F<sub>0.1</sub>. The arrows indicate  $T_c$ . The broken straight lines show the relation  $1/T_1 \propto T$ , and the curves below  $T_c$  are fits to the BCS model with the gap size indicated in the figure.

the increasing is very small. The  $1/T_1 T$  of stoichiometric LiFeAs is almost constant. While  $1/T_1 T$  of LaNiAsO<sub>0.9</sub>F<sub>0.1</sub> decrease with decreasing temperature. These results suggest that the antiferromagnetic spin fluctuations are stronger in Ba<sub>0.72</sub>K<sub>0.28</sub>Fe<sub>2</sub>As<sub>2</sub> and LaFeAsO<sub>0.92</sub>F<sub>0.08</sub>, but quite weak in LiFeAs and LaNiAsO<sub>0.9</sub>F<sub>0.1</sub>. This difference may be understood by the difference of the Fermi surface topology. There are not only hole-pockets and electron-pockets but also nesting between them in Ba<sub>0.72</sub>K<sub>0.28</sub>Fe<sub>2</sub>As<sub>2</sub> and LaFeAsO<sub>0.92</sub>F<sub>0.08</sub>, which can promote spin fluctuations. While in LiFeAs there is no such nesting, although there are still hole-pockets and electron-pockets. Lacking of such nesting make the spin fluctuation become weaker than Ba<sub>0.72</sub>K<sub>0.28</sub>Fe<sub>2</sub>As<sub>2</sub> and LaFeAsO<sub>0.92</sub>F<sub>0.08</sub>. In LaNiAsO<sub>0.9</sub>F<sub>0.1</sub> there is no hole-pockets, then nesting can not happen, therefore the spin fluctuations are not expected.

Finally, we discuss the anisotropy of the spin fluctuations. In a general form,  $1/T_1 T$  is written as

$$\frac{1}{T_1 T} = \frac{\pi k_B \gamma_n^2}{(\gamma_e \hbar)^2} \sum_q A_{hf}^2 \frac{\chi''_{\perp}(q, \omega)}{\omega}, \quad (5)$$

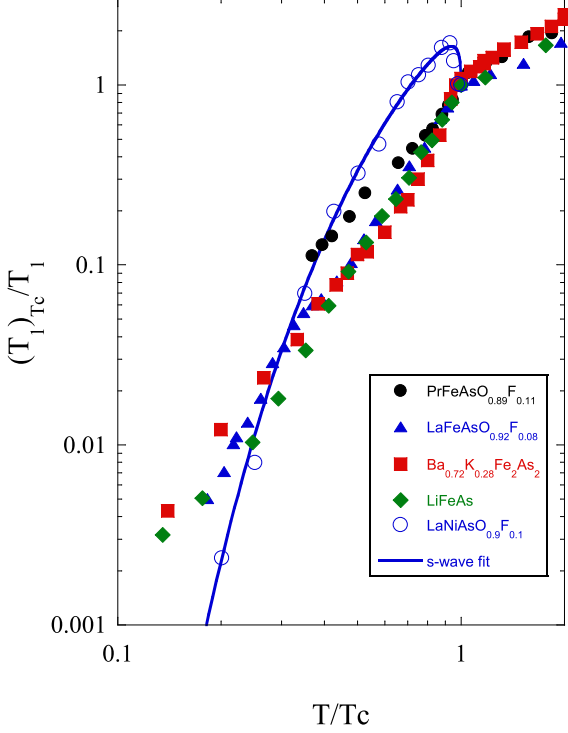


Figure 8: (color online) The normalized T-dependence of  $1/T_1$  for  $\text{PrFeAsO}_{0.89}\text{F}_{0.11}$  ( $T_c = 45$  K),  $\text{LaFeAsO}_{0.92}\text{F}_{0.08}$  ( $T_c = 23$  K),  $\text{Ba}_{0.72}\text{K}_{0.28}\text{Fe}_2\text{As}_2$  ( $T_c = 31.5$  K),  $\text{LiFeAs}$  ( $T_c = 17$  K),  $\text{LaNiAsO}_{0.9}\text{F}_{0.1}$  ( $T_c = 4.0$  K).

where  $\chi''(q, \omega)$  is the imaginary part of the dynamical susceptibility perpendicular to the applied field. The anisotropic ratio in the form of  $\frac{\sum_q A_{hf}^c(q)^2 \chi''(q)}{\sum_q A_{hf}^a(q)^2 \chi''(q)}$  for  $\text{Ba}_{0.72}\text{K}_{0.28}\text{Fe}_2\text{As}_2$  and parent compound are shown in Fig.11. The larger magnitude of  $1/T_1 T$  along the  $a$ -axis direction than that along the  $c$ -axis direction indicates that there are stronger fluctuations along the  $c$ -axis direction seen by the As-site. Neutron experiment found that, in the undoped  $\text{BaFe}_2\text{As}_2$  compound, the ordered Fe magnetic moment is along the  $a$ -direction and forms a stripe [29]. Since the As atom sits in the position above (below) the middle of four Fe-atoms, our result implies that, in the Fe site, a stronger fluctuating fields exist along the  $a$ -axis direction, as illustrated in the inset of Fig. 9. It is remarkable that the antiferromagnetic fluctuations of Fe are anisotropic in spin space. Namely,  $\chi''_{\pm}(Q)$  is much larger than  $\chi''_{zz}(Q)$ , where  $z$  is along the  $c$ -axis direction and  $Q$  is the spin fluctuation wave vector. This is in contrast to the high- $T_c$  cuprates where the spin fluctuations are believed to be isotropic, but similar situation was encountered in cobaltate superconductor [30]. The relationship between the energy- and  $q$ -dependence of the spin fluctuations (SF) and possible SF-induced superconductivity has been studied both theoretically [31] and experimentally [32]. To our knowledge, however, the relationship between the anisotropy of SF and superconductivity has been less explored so far. We hope that our results will stimulate more theoretical work in this regard.

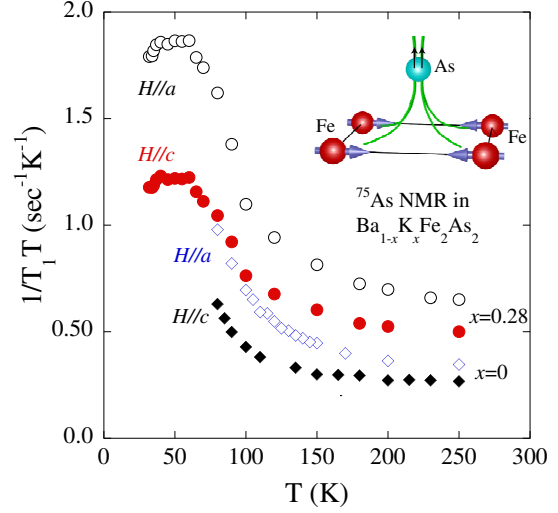


Figure 9: (color online) The quantity  $^{75}(1/T_1 T)$  in the normal state of  $\text{Ba}_{0.72}\text{K}_{0.28}\text{Fe}_2\text{As}_2$  (circles) and in the paramagnetic state of  $\text{BaFe}_2\text{As}_2$  (diamonds). The arrows in the inset illustrate the larger component of the fluctuating field of Fe and that seen by the As site.

#### 4. Conclusion

In summary, we have presented the NMR and NQR results on the electron-doped Fe-arsenides  $\text{PrFeAsO}_{0.89}\text{F}_{0.11}$  ( $T_c = 45$  K),  $\text{LaFeAsO}_{0.92}\text{F}_{0.08}$  ( $T_c = 23$  K), stoichiometric  $\text{LiFeAs}$  ( $T_c = 17$  K), and the hole-doped Fe-arsenide  $\text{Ba}_{0.72}\text{K}_{0.28}\text{Fe}_2\text{As}_2$  ( $T_c = 31.5$  K). We find there are multiple gaps in iron arsenides where Knight shift and  $1/T_1$  does not follow a simple power-law nor exponential function. However, the  $1/T_1$  of the Nickel analog  $\text{LaNiAsO}_{0.9}\text{F}_{0.1}$  shows a well-defined coherence peak just below  $T_c$  and an exponential behavior at lower temperatures. These properties indicate that it is a conventional BCS superconductor. The difference between the Fe-arsenides and the Ni-analog may be understood by the difference of the Fermi surface topology, and therefore highlights the important role of the Fermi-surface topology in pairing symmetry of the iron arsenides superconductors.

In the normal state, all iron arsenides show weak antiferromagnetic spin correlations. Our data also show that the sample with weaker correlations has a lower  $T_c$ , and this may imply the  $T_c$  has a relationship with the structure of Fermi surface. Moreover, the spin fluctuations are anisotropic in spin space, which is different from cuprates.

We gratefully acknowledge the support from CAS, National Science Foundation of China, JSPS and MEXT of Japan.

#### References

- [1] Y. Kamihara *et al*, J. Am. Chem. Soc. **130**, 3296 (2008).
- [2] Z. -A. Ren *et al*, Chin. Phys. Lett. **25**, 2215 (2008).
- [3] M. Rotter *et al*, Phys. Rev. Lett. **101**, 107006 (2008).
- [4] X. C. Wang *et al*, Solid State Commun. **148**, 538 (2008).
- [5] Z.-A. Ren *et al*, Materials Research Innovations **12**, 105 (2008).
- [6] G. F. Chen *et al*, Phys. Rev. Lett. **101**, 057007 (2008).
- [7] Z. Li *et al*, Phys. Rev. B **78**, 060504(R) (2008).
- [8] G.L. Sun *et al*, arXiv:0901.2728 (2009).

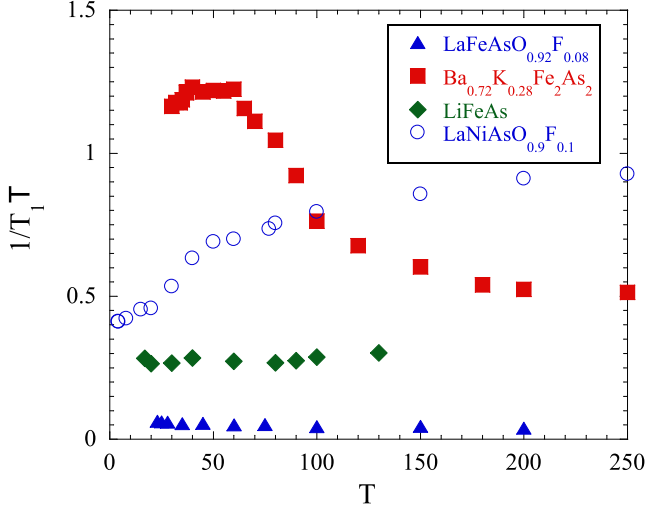


Figure 10: (color online) The T-dependence of  $1/T_1 T$  for  $\text{LaFeAsO}_{0.92}\text{F}_{0.08}$  ( $T_c=23$  K),  $\text{Ba}_{0.72}\text{K}_{0.28}\text{Fe}_2\text{As}_2$  ( $T_c = 31.5$  K),  $\text{LiFeAs}$  ( $T_c = 17$  K),  $\text{LaNiAsO}_{0.9}\text{F}_{0.1}$  ( $T_c = 4.0$  K).

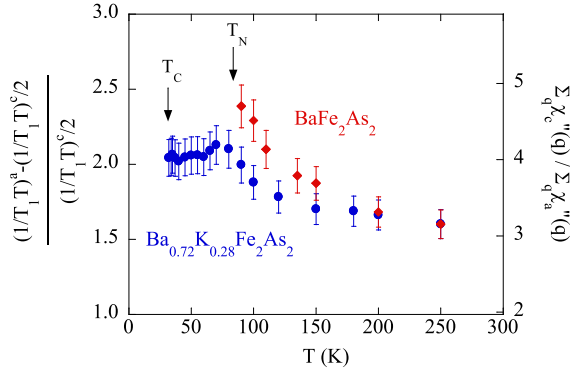


Figure 11: (color online) The T dependence of the anisotropy of the spin fluctuations seen at the As site in terms of  $\frac{\sum_{\mathbf{q}} A_{hf}^c(\mathbf{q})^2 \chi''_c(\mathbf{q})}{\sum_{\mathbf{q}} A_{hf}^a(\mathbf{q})^2 \chi''_a(\mathbf{q})}$  for the left axis and  $\frac{\sum_{\mathbf{q}} \chi''_c(\mathbf{q})}{\sum_{\mathbf{q}} \chi''_a(\mathbf{q})}$  for the right axis.

- [30] K. Matano *et al*, Europhys. Lett. **84**, 57010 (2008).
- [31] T. Moriya and K. Ueda, J. Phys. Soc. Jpn. **63**, 1871 (1994); D. Monthoux and D. Pines, Phys. Rev. B **49**, 4261 (1994).
- [32] G.-q. Zheng *et al*, J. Phys. Soc. Jpn. **64**, 3184 (1995).

- [9] K. Matano *et al*, Europhys. Lett. **83**, 57001 (2008).
- [10] K. Matano *et al*, Europhys. Lett. **87**, 27012 (2009).
- [11] S. Kawasaki *et al*, Phys. Rev. B **78**, 220506 (R) (2008).
- [12] I. I. Mazin *et al*, Phys. Rev. Lett. **101**, 057003 (2008).
- [13] K. Kuroki *et al*, Phys. Rev. Lett. **101**, 087004 (2008).
- [14] A.V. Chubukov *et al*, Phys. Rev. B **78**, 134512 (2008). D. Parker *et al*, *ibid*, 134524 (2008). M. M. Parish *et al*, *ibid*, 144514 (2008).
- [15] Y. Bang and H. -Y. Choi, Phys. Rev. B **78**, 134523 (2008); Y. Nagai *et al*, New J. Phys. **10**, 103026 (2008).
- [16] Z. Li *et al* J. Phys. Soc. Jpn. **79**, 083702 (2010).
- [17] X. C. Wang *et al*, Solid State Commun. **148**, 538 (2008) J. H. Tapp *et al*, Phys. Rev. B **78**, 060505 (2008).
- [18] D.J. Singh and M. H. Du, Phys. Rev. Lett. **100**, 237003 (2008).
- [19] T. Tabuchi *et al*, Phys. Rev. B **81**, 140509 (2010).
- [20] Y. Nakai *et al*, J. Phys. Soc. Jpn. **77**, 073701 (2008).
- [21] H.-J. Grafe *et al*, Phys. Rev. Lett. **101**, 047003 (2008).
- [22] H. Fukazawa *et al*, J. Phys. Soc. Jpn. **78**, 033704 (2009).
- [23] L. C. Hebel, Phys. Rev. **116**, 79 (1959).
- [24] S. Graser *et al*, New J. Phys. **11**, 025016 (2009).
- [25] K. Kuroki *et al*, Phys. Rev. B **79**, 224511 (2009).
- [26] G. Xu *et al*, Europhys. Lett. **82**, 67002 (2008) .
- [27] G.-q. Zheng *et al*, Phys. Rev. Lett. **90**, 197005 (2003).
- [28] G. - q. Zheng *et al*, Phys. Rev. B **73**, 180503 (R) (2006).
- [29] Q. Huang *et al*, , Phys. Rev. Lett. **101**, 257003 (2008)